A structural study of a C_3H_3 species coadsorbed with CO on Pd(111)

M. J. Knight[1], F. Allegretti[1×], E. A. Kröger[2], M. Polcik[2♦], C. L. A. Lamont[3], D. P. Woodruff[1*]

[1] *Physics Dept, University of Warwick, Coventry CV4 7AL, UK*

[2] *Fritz-Haber-Institut der Max-Planck-Gesellschaft, Faradayweg 4-6, 14195 Berlin, Germany*

[3] *Dept. of Chemical & Biological Sciences, University of Huddersfield, Queensgate, Huddersfield HD1 3DH, UK*

Abstract

The combination of chemical-state-specific C 1s scanned-energy mode photoelectron diffraction (PhD) and O K-edge near-edge X-ray absorption fine structure (NEXAFS) has been used to determine the local adsorption geometry of the coadsorbed C_3H_3 and CO species formed on Pd(111) by dissociation of molecular furan. CO is found to adopt the same geometry as in the Pd(111)c(4x2)-CO phase, occupying the two inequivalent three-fold coordinated hollow sites with the C-O axis perpendicular to the surface. C_3H_3 is found to lie with its molecular plane almost parallel to the surface, most probably with the two 'outer' C atoms in equivalent off-atop sites, although the PhD analysis formally fails to distinguish between two distinct local adsorption sites.

Keywords: Surface structure; photoelectron diffraction; palladium; furan; hydrocarbons

---

[×] present address: Karl-Franzens-Universität Graz, Institut für Physik, Bereich für Experimentalphysik, Universitätsplatz 5, 8010 – Graz, Austria

[♦] present address: ANF Data, AS IL W, Herspicka 5, 639 00, Brno, Czech Republic

[*] corresponding author: email d.p.woodruff@warwick.ac.uk

1. Introduction

Much of the motivation of ultra-high vacuum surface science studies of the interaction of molecules with solid surfaces is to understand the elementary steps involved in surface reactions, particularly those involved in heterogeneous catalysis, and as such the identification and characterisation of surface intermediate species is an important goal. Very few of these surface species have been investigated by quantitative structural methods, the main exceptions to this statement being deprotonated alcohols and carboxylic acids [1], although there have also been a few investigations of one novel surface hydrocarbon species, ethylidyne (CH_3-C-) [2, 3]. Here we present the results of an investigation aimed at elucidating the local structure of a C_3H_3 surface species which is believed to occur, coadsorbed with CO, on Pd(111) as a result of thermal dissociation of adsorbed furan.

Furan, C_4H_4O, is the simplest oxygen-containing aromatic hydrocarbon, and is often used as a model in hydrodeoxygenation studies of such compounds that need to be removed from crude petroleum and liquids derived from coal and biomass [4]. Several surface science investigations have established that on Pd(111) furan adsorbs intact at low temperatures, but at around room temperature dissociation occurs with the production of coadsorbed species identified as CO and C_3H_3 [5, 6, 7]. Evidence for these assignments comes from several different techniques. Temperature programmed desorption (TPD) shows a peak for molecular H_2 at ~350 K, characteristic of H-H recombination on Pd(111), indicating that atomic H is released from the furan below ~300 K [5]. CO desorption is seen at a higher temperature of ~500 K, also consistent with desorption being the rate-limiting process, and thus with its creation on the surface at a lower temperature [5]. The C 1s photoelectron binding energy in X-ray photoelectron spectroscopy (XPS), ultra-violet photoelectron spectroscopy (UPS) data, and the appearance of a vibrational band in high-resolution electron energy loss spectroscopy (HREELS) at ~1800 cm^{-1}, all provide identification of the presence of molecular CO on the surface after the initial dissociation [5]. Both XPS and HREELS data also provide

direct support for the view that the coadsorbed species is a hydrocarbon. Perhaps the most direct evidence that this species is correctly identified as C_3H_3 comes from laser-induced thermal desorption (LITD), which shows a small yield of molecular benzene, C_6H_6, above ~350 K that can be attributed to coupling of a C_3H_3 surface intermediate. No benzene desorption is produced in the gas phase by conventional TPD as this molecule dissociates on Pd(111) on heating, but LITD achieves very rapid heating that can favour direct desorption [6, 7]. A more recent study of intact molecular furan adsorption at low temperatures by scanning tunnelling microscopy (STM) [8, 9] has also been extended to investigate the room temperature dissociation products and a distinct molecular species on the surface (as imaged in STM, including theoretical simulations of the STM images using extended Hückel theory) has been attributed to this C_3H_3 species [10].

Here we report on the results of an experimental quantitative structure investigation of these coadsorbed molecular fragments adsorbed on Pd(111) using the technique of scanned-energy mode photoelectron diffraction (PhD) [11, 12], combined with near-edge X-ray absorption fine structure (NEXAFS). O K-edge NEXAFS provides information on the molecular orientation of the CO, while chemical-state-specific C 1s PhD provides information on the local registry and adsorbate-substrate bondlengths of the two coadsorbed species. The results show that the CO molecules have local adsorption geometries closely similar to those in the absence of the coadsorbed C_3H_3, but provide entirely new information on the adsorption geometry of this novel species.

2. Experimental details and surface characterisation

The experiments were conducted in an ultra-high vacuum surface science end-station equipped with typical facilities for sample cleaning, heating and cooling. This instrument was installed on the UE56/2-PGM-2 beamline of BESSY II which comprises a 56 mm period undulator followed by a plane grating monochromator [13]. Different electron emission directions can be detected by rotating the sample about its surface normal (to change the azimuthal angle) and about a vertical axis (to change the polar angle). Sample characterisation *in situ* was achieved by low energy electron diffraction (LEED) and by

X-ray photoelectron spectroscopy (XPS) using both Mg K_α radiation and the incident synchrotron radiation (SXPS). Both the wide-scan photoemission spectra for surface characterisation, and the narrow-scan O 1s and C 1s spectra recorded in the PhD measurements, were obtained using an Omicron EA-125HR 125 mm mean radius hemispherical electrostatic analyser. This was equipped with seven-channeltron parallel detection, and was mounted at a fixed angle of 60° to the incident monochromated synchrotron radiation in the same horizontal plane as that of the polarisation vector of the radiation.

A clean well-ordered Pd(111) surface was prepared from an oriented and polished crystal slice by the usual combination of cycles of 1 keV Ar ion bombardment and brief annealing to 900 K to give a sharp (1x1) LEED pattern and XPS/SXPS spectra devoid of impurities. Some residual carbon that appeared after successive furan dosing experiments and proved rather resistant to Ar ion bombardment was removed by heating the sample to ~750 K in a partial pressure of $5x10^{-9}$ mbar of oxygen, the surface then being heated briefly to 900 K in UHV to remove the surface oxygen. Furan dosing from the vapour was performed at a sample temperature of 90-120 K, the gas-phase purity being checked by mass spectrometry during the dosing. Typical exposures were $6x10^{-6}$ mbar.s, followed by brief heating to ~160 K to desorb any possible multilayer components. Fig. 1 shows typical C 1s SXPS spectra which clearly show two distinct components, the energies of which differ after heating to successively higher temperatures. As we are concerned here only with identifying different species through relative binding energy shifts, these spectra are plotted in terms of nominal kinetic energy and no absolute calibration of the associated binding energies was undertaken. While the spectral resolution is greatly superior to the earlier XPS data obtained from a conventional laboratory-based instrument [5], the trends are clearly the same and are consistent with the intact furan molecule reacting to form coadsorbed CO and C_3H_3 in the temperature range from ~230-300 K [5, 6]. At low temperatures the two peaks in Fig. 1 can be associated with the two inequivalently-located C atoms within the furan molecule; as in previous work we attribute the lower kinetic energy (higher binding energy) state to the C atoms bonded to oxygen (the so-called α-C atoms), while emission from the C atoms bonded only to C

and H (the β-C atoms), is the source of the higher kinetic energy (lower binding energy) peak. At high temperatures the low and high binding energy components are attributed to the C_3H_3 and CO fragments, respectively. The higher binding energy peak at low temperature has an appearance suggestive of two unresolved components that may be attributed to the presence of small amounts of coadsorbed CO; this effect was also noted in the earlier work of Caldwell and Land [14]. The apparent asymmetry of the low binding energy peak in the high-temperature phase, assigned to the C_3H_3 species, may also be due to some inequivalence of the three constituent C atoms, but no reliable separation of the hydrocarbon peak into two (or more) components for separate PhD analysis could be achieved, although this hydrocarbon component peak is significantly wider than that associated with the CO. Indeed, satisfactory fits to the PhD C 1s spectra from the surface following furan dissociations were obtained using just two symmetric Gaussian peaks, albeit of different widths; for example at a kinetic energy of ~60 eV the FWHM values of the CO and C_3H_3 peaks were found to be 0.58 eV and 1.02 eV respectively. A matching set of O 1s spectra was also collected, but the overlap of the strong Pd $3p_{3/2}$ substrate emission peak renders these spectra rather uninformative, though there clearly are binding energy shifts on heating attributable to the conversion from adsorbed furan to adsorbed CO. For the PhD measurements of the CO/C_3H_3 coadsorption phase reported here, the furan-dosed surface, prepared as described above, was gently heated to 340 K and then cooled to the measurement temperature of ~120 K.

The PhD technique [11, 12] exploits the coherent interference of the directly-emitted component of the outgoing photoelectron wavefield from a core level of an adsorbate atom with components of the same wavefield which are elastically backscattered by the nearby substrate atoms. By measuring the photoemission intensity in specific directions as a function of photon energy, the resulting changes in photoelectron energy, and thus photoelectron wavelength, cause specific scattering paths to switch in and out of phase with the directly-emitted component, leading to modulations in the intensity which depend on the relative emitter-scatterer location. These PhD modulation spectra were obtained by recording a sequence of photoelectron energy distribution curves (EDCs) around the C 1s peaks at 4 eV steps in photon energy in the photoelectron kinetic energy

range of approximately 50 to 250-300 eV for each of a number of different emission directions. The upper energy of this range on Pd substrates is limited by the problems of intense Pd Auger electron emission peaks which are difficult to separate reliably from the C 1s photoemission signal when the energies overlap. Such spectra were recorded in a total of 13 different emission directions, namely 0° (normal emission), 10°, 30°, 50° and 60° in the $[\bar{1}2\bar{1}]$ azimuth, 10°, 30°, 50° and 70° in $[\bar{1}10]$, and 10°, 20°, 40° and 50° in $[\bar{2}11]$; these azimuthal directions are defined in Fig. 2. These data were processed following our general PhD methodology (e.g. [11, 12]) in which the individual EDCs are fitted by the sum of Gaussian peaks, a step and a template background. The integrated areas of each of the two C 1s chemically-shifted component peaks were then plotted as a function of photoelectron energy and each final PhD modulation spectrum was obtained by subtraction of, and normalisation by, a smooth spline function representing the non-diffractive intensity and instrumental factors. Notice that this procedure leads to meaningful *absolute* modulation amplitudes, which are matched in absolute terms by the multiple scattering simulations of the model structures. The resulting two sets of PhD modulation spectra, one for the C emitter atom in CO, the other for the C emitter atoms in C_3H_3, were used in the structure analysis described in the following section.

O K-edge NEXAFS spectra were recorded in the Auger electron detection mode by measuring the intensity of the electron emission at the energy corresponding to the O KVV Auger transition (513 eV), and scanning the photon energy through the O K-edge. Spectra were recorded at a range of angles of incidence from normal to grazing; these changes in incidence geometry provide information on the dependence of the intensity of the molecular resonance peaks on the direction of the polarisation vector of the linearly-polarised incident radiation. These data provide the basis for a determination of the molecular orientation of the adsorbed CO.

3. Results and data analysis

3.1 CO

Fig. 3 shows the set of O K-edge NEXAFS spectra recorded from the CO, coadsorbed

with C_3H_3, on Pd(111). The measurements were made at a series of different incidence angles; using the usual NEXAFS nomenclature, these angles, θ_E, correspond to the grazing incidence angle (i.e. θ_E=90º corresponds to normal incidence). Notice that (see fig. 3), because of the geometry of the experiment, using horizontally-polarised radiation, θ_E also corresponds to the angle between the polarisation vector of the radiation and the surface normal. The spectra of Fig. 3 show two particularly clear and intense resonance peaks at nominal (uncalibrated) photon energies of ~532 eV and 547 eV that correspond, respectively, to the well-known π^* and σ^* final state resonances of molecular CO. The general trend of the changes in amplitude of these two peaks with variations in the incident geometry are consistent with the expected molecular orientation with the C-O axis essentially perpendicular to the surface; this is the orientation of CO on Pd(111) in the absence of coadsorbates [15, 16]. In particular, the π^* resonance has its maximum intensity at normal incidence (*E*-vector parallel to the surface and thus perpendicular to the molecular axis), while this incidence geometry leads to minimisation of the intensity of the σ^* resonance. These qualitative arguments can be made more quantitative by exploiting the well-known and simple formulae describing the polarisation-angle dependence of the two types of final state resonance [17, 18]. To do so one must extract the relative intensities of the resonance peaks by fitting the individual NEXAFS spectra to a step, representing the edge-jump in the atomic photoionisation cross-section, and a consistent set of peaks representing the various distinct final states. This procedure is substantially more reliable for the π^* resonance peak, which is narrow and appears right at the adsorption edge, although even for this peak the assumption regarding the size of the edge-jump impacts on the measured intensity, particularly at grazing incidence. However, the σ^* resonance occurs in an energy range in which there are other rather indistinct features, probably associated with scattering of the photoelectrons by substrate atoms, so in this range extracting reliable intensities is even more difficult. We therefore report here only the results of this analysis applied to the π^* resonance peak, for which we find the best fit to the data corresponds to an angle of the C-O axis relative to the surface normal, γ, of 0°, i.e. with the molecular axis perpendicular to the surface. A typical error estimate for this type of NEXAFS analysis is no better that ±10º, as reflected in the different theoretical curves shown in the inset diagram of Fig. 3. Note that this inset

figure was obtained from fitting which placed the edge jump at 520.2 eV, just below the energy of the π^* resonance peak; an alternative fitting, with the edge jump at 535.1 eV just above the π^* resonance, led to relatively small changes, the best-fit tilt angle being approximately 10° in this case.

Whilst this NEXAFS analysis provides information on the CO molecular orientation, the local adsorption site and associated bondlengths must be extracted from the PhD data. As described in section 2, an extensive set of C 1s PhD spectra were collected in 13 different directions. Our standard methodology in the PhD technique is then to select for detailed analysis, a subset of these, concentrating on those spectra that show the strongest modulations, but with the added constraint that a reasonable range of emission geometries should be included. For the CO data our structural analysis is based on a set of 8 PhD spectra recorded at polar emission angles from normal emission to 40°.

Structure determination in the PhD technique is based on the same trial-and-error approach used in quantitative LEED studies, whereby multiple scattering calculations are performed of the PhD spectra to be expected from a range of different model structures, the detailed structural parameter values then being iterated to achieve the best agreement between theory and experiment. The quality of agreement between theory and experiment is judged by the value of an objective reliability- or *R*-factor, defined as a normalised summation of the squares of the differences between the (absolute) experimental and theoretical modulation amplitudes at each point in the spectra [11, 12]. Some 'space-scanning' searches of parameter space involve calculations over a grid of parameter values. Other searches, particularly to optimise specific structural models to locate the structure having the minimum *R*-factor, are performed with the help of an adaptation of the original Newton-Gauss method [19] which uses a later implementation of a Marquardt algorithm [20], in which the calculation of the curvatures is made considerably faster by using the so-called liner method [21]. Optimisation of the fit between theory and experiment involves mainly adjustment of structural parameter values, but also of vibrational amplitudes of both emitter and scatterer atoms, together with the inner potential. (The typical value of the inner potential used here was 17 eV;

note this parameter also accounts for instrumental effects and contact potential differences.) If the *R*-factor value of the best-fit (lowest *R* value) structure is acceptably low, the associated model structure is then believed to be a true representation of the surface structure. The magnitude to be regarded as acceptably low does depend on the type of system studied; for structures involving occupation of a single high-symmetry site on a surface, values of 0.20 or less are often achieved, but with multiple site occupation or low-symmetry sites, the PhD modulations are generally much weaker and significantly higher minimum *R*-factors (up to 0.40 or even higher) may be found. The calculations were performed with computer codes developed by Fritzsche [21, 22, 23, 24] that are based on the expansion of the final state wave-function into a sum over all scattering pathways that the electron can take from the emitter atom to the detector outside the sample.

Models involving CO adsorption in all the most symmetric adsorption sites were tested, namely atop, bridge and the two inequivalent three-fold coordinated hollow sites, the so-called ‘fcc’ and 'hcp’ hollows (above third and second layer substrate atoms, respectively). At each site a range of values of the local structural parameters (most notably the height of the C atoms above the outermost Pd atomic layer), but also the C-O distance, the outermost Pd layer spacing, and the vibrational amplitudes of the emitter and scatterer atoms, were explored. In all cases the C-O axis was assumed to be perpendicular to the surface, as indicated by the NEXAFS results. In addition to these four distinct single-occupied sites, additional calculations based on equal co-occupation of all possible pairs of these sites were conducted. For the single-site models the lowest *R*-factor values found were 0.67 (atop), 0.44 (bridge), 0.26 (fcc hollow), and 0.34 (hcp hollow), clearly favouring the fcc hollow site. However, the model involving co-occupation of the fcc and hcp sites yielded a substantially lower value of R=0.18. The only other co-occupation model yielding a lower *R*-factor value than the best single-site model was that involving a mixture of fcc hollow and bridge sites, but the value obtained (R=0.24) is significantly larger than that of the best-fit mixed-hollow model. Specifically, in order to determine the uniqueness of a solution to a PhD analysis, and to estimate the errors associated with the individual structural parameters, we define a variance in the

minimum of the *R*-factor, R_{min}, following an approach developed by Pendry for LEED [25]. Specifically, $Var(R_{min}) = (R_{min})\sqrt{(2/N)}$ where N is the number of independent pieces of structural information contained in our experimental spectra; as in Pendry's LEED work, N is obtained from a ratio of the total energy range of the PhD spectra and a characteristic peak width, described more fully elsewhere [26]. (In the investigation described here the values of N were 56 and 41 for the CO and C_3H_3 analyses, respectively). All parameter values giving structures with *R*-factors less than R_{min}+ $Var(R_{min})$ are regarded as falling within one standard deviation of the 'best fit' structure . In the present case the lowest *R*-factor value is 0.18, and the variance is 0.03, so we can formally exclude all structures yielding *R*-factor values greater than 0.21. Fig. 4 shows a comparison of the experimental PhD spectra and the theoretical simulations for this best-fit structure, while the associated structural parameter values and their estimated precision is shown in Table 1. Also shown in Table 1 are the structural parameters obtained in earlier analyses of pure CO adsorption phases on Pd(111), also performed using the PhD technique [15, 16].

3.2 C_3H_3

For the C_3H_3 species our structure determination relies entirely on the PhD technique; O K-edge NEXAFS provides no information on the C_3H_3 species, and the use of C K-edge NEXAFS presents both technical problems and difficulties in interpretation. In particular, C contamination in the beamline optics makes it difficult to obtain reliable data, while separating the NEXAFS signals from the CO and C_3H_3 coadsorbates in a reliable fashion through the use of difference spectra would present a significant challenge. In all emission geometries the C 1s PhD spectra showed only weak modulations; most spectra showed modulation amplitudes of less than ±10%. Bearing in mind the fact that the interatomic C-C distances within the molecule must differ from the Pd-Pd distances in the Pd(111) surface, it is inevitable that the individual C atoms occupy low-symmetry sites on the surface. As a result, the PhD spectra comprise an incoherent sum of all such geometries that are symmetrically-equivalent relative to the substrate. Relatively weak PhD modulations are therefore to be expected. However, very weak modulations present

a challenge to both the theoretical description and the experimental reliability, so it is particularly important in this case that the PhD structure determination should be performed using those spectra that show the strongest modulations, nevertheless applying the added constraint that a reasonable range of emission geometries should be included. On this basis our structural analysis is based on a subset of 6 PhD spectra, mainly near normal emission, but including two spectra at 30º and 40º polar emission angles.

For the C_3H_3 species even the molecular conformation is unknown. Perhaps the most obvious configuration is to regard this species as one half of a benzene molecule, in which case one might consider bonding to the surface through two of the three C atoms in a triangular configuration with the molecular plane perpendicular to the surface (as though bonding to the missing half of the benzene). However, as benzene itself typically lies flat on metal surfaces, bonding through its π-electron system, one may also consider that there may also be some forces favouring an orientation of the triangular molecular plane more nearly parallel to the surface. Of course, the actual C-C-C angle within either of these bonding configurations is unknown, the extreme (and improbable) case being an angle of 180º such as to produce a linear species. In any of these scenarios, however, one might expect two of the three C atoms to occupy sites that are at the same height above the surface, and are quite possibly symmetrically equivalent, while the third C atom at the apex of the triangle must then occupy a fundamentally different site. This discussion highlights the fact that for most geometries the measured experimental modulations may be dominated by the PhD from the two (near-) equivalent C atoms, with the modulations from the third atom leading to partial cancellation and partial reinforcement arising from the other two atoms. For this reason, an initial search of the PhD modulations to be expected from a single C atom at all possible sites on the surface may be expected to provide some clue to the optimum molecular geometry. This initial 'space-scanning' search of single C 1s emitter sites in high-symmetry directions, (performed using multiple scattering calculations with a reduced number of scattering events of ~800 single scattering, ~250 double scattering and ~100 triple scattering pathways), did identify a number of possible sites which gave reasonable agreement with the set of experimental PhD modulation spectra (*R*-factor values in the range ~0.3-0.4), mostly involving off-

atop sites about 2.0-2.1 Å above the outermost Pd atomic layer.

Based, in part, on this information, more realistic calculations, using a similar number of scattering pathways but including all three C emitter atoms, were performed for a number of reasonably symmetric structural models. These basic models are illustrated in fig. 5; the H atoms are omitted from the calculations (and the figure) as they are extremely weak electron scatterers. In all cases the initial models are loosely based on a molecular conformation equivalent to that of one half of a benzene molecule, but the choice of the structures tested was also influenced by the results of the single emitter atom calculations. These calculations explored C-C-C angles in the range 80-125º and C-C bondlengths from 1.3-1.5 Å. In models 1 to 4 (fig. 5) the molecular plane is assumed to be perpendicular to the surface. Models 2 and 3 place the molecule directly atop a surface Pd atom in the two highest-symmetry azimuths, while in models 1 and 4 the molecule is centred over a bridging site with symmetric azimuthal orientations corresponding, respectively, to aligned-bridge and cross-bridge geometries. By contrast models 5, 6 and 7 are based on an initial assumption that the molecular plane is parallel to the surface. In models 6 and 7 the C_{2v} axis of the molecule is aligned in the <211> mirror planes, with the central C atoms being located in the vicinity of fcc and hcp hollow sites, respectively. In model 5 the C_{2v} molecular axis is aligned along a <110> close-packed direction of the surface. For each of these models a range of structural parameters were varied to locate the values corresponding to the lowest *R*-factors. For the perpendicular orientations, models 1-4, the central C atom was kept in the symmetric atop or bridge site, but was allowed to take different heights above the surface, while the outer C atoms were allowed to move both perpendicular and parallel to the surface. These movements of the outer C atoms were constrained to retain the common mirror symmetry of the molecule and the outermost substrate layer, and the perpendicular molecular orientation. For models 5-7, lateral movements of both the outer and central C atoms were permitted, but with the central C atom moving only within the <110> (model 5) or <211> (models 6 and 7) azimuths from the original models. For these lying-down molecular configurations, the fact that the central and outer C atoms were allowed to move, independently, perpendicular to the surface, also meant that the molecule could tilt out of its initial

parallel orientation. In addition to all these individual models, one further model, model 8, in which equal occupation of sites 6 and 7 was assumed, allowed us to test the possibility that occupation of the fcc and hcp hollow sites is equally probable. For all models, optimisation of the vibrational amplitudes was also undertaken.

The results of these initial structural optimisations are summarised in Table 2. A striking conclusion is that the four models (numbers 5-8) in which the molecular plane is approximately parallel to the surface yield *R*-factor values that are very significantly lower than any of the models in which the molecular plane is perpendicular to the surface. The variance in the minimum value of the *R*-factor of 0.20 is calculated to be 0.04, so formally we can reject all models for which $R>0.24$. Notice, too, that the structure having a perpendicular orientation with the lowest *R*-factor (model 4, $R=0.30$) has unreasonably long C-C bondlengths of 1.67 Å.

In a second stage of structural searches, a number of the symmetry constraints applied in the initial stage were relaxed, and the automated structural optimisations were undertaken using different initial parameter values to check for global, rather than local, *R*-factor minima. This stage focussed on models 5-8, but also included model 1, the most promising of the models based on a molecular orientation perpendicular to the surface that yielded realistic C-C bondlengths. For model 1, additional modifications tested the effect of permitting a twist about the perpendicular molecular C_{2v} axis, or of a tilt of the molecule away from its initial perpendicular configuration, either keeping the outer C atom positions fixed, or allowing them to move parallel to the surface. These reduced constraints only led to a reduction of the *R*-factor to 0.27, still well outside the range of acceptable values defined by the models based on a molecular plane close to parallel to the surface. We therefore conclude that none of the models based on the molecular plane being perpendicular, or near-perpendicular, to the surface, lead to acceptable structures. As models 6, 7 and 8 differ only with respect to the relative location of second (and deeper) layer Pd atoms, and appear to yield identical *R*-factor values, we then concentrated on testing the optimisation of models 5 and 8 more thoroughly, checking particularly to distinguish local and global minima. This process failed to find better

structural solutions – new variations of models 5 and 8 were found, but with higher *R*-factor values in the range 0.24-0.26, evidently corresponding to local minima in the structural parameter space.

Final structural calculations for models 5 and 8 were then undertaken using a significantly larger number of scattering pathways to ensure convergence, and re-optimising all parameters under these conditions. The *R*-factor values resulting from this process are slightly higher, at 0.20 for model 5 and 0.23 for model 8. The structural parameter values obtained for these two structures are summarised in Table 3, while the comparisons of the experimental modulation spectra with the results of these two calculations are shown in fig. 6. The specific structures are shown schematically in Fig. 7. Table 3 includes error estimates for all the parameter values based on the calculated variance of the minimum *R*-factor, as described above. Notice that the precision in the location of the C atoms is higher for the near-atop C emitters (the centre C in model 5 and the outer C atoms in model 8), as these contribute stronger modulations to the PhD spectra recorded near normal emission. A second factor is that for locally equivalent geometries, the precision in the location of the outer C atoms (of which there are two) is typically better than of the centre atom; thus, the precision of the location of the off-hollow outer C atom in model 5 is better than that of the similarly-located single centre atom in model 8. The values in Table 3 also reflect the typical characteristic of PhD data in showing better precision in distances perpendicular to the surface than parallel to the surface.

4. General Discussion and Conclusions

Our structural conclusions regarding the local adsorption geometry of CO on Pd(111), when coadsorbed with C_3H_3, hold no great surprises. In the absence of the coadsorbed hydrocarbon, CO appears to prefer to occupy the fcc hollow site, which it does to the exclusion of all other sites at a coverage of 0.33 ML, in the ordered (√3x√3)R30º-CO phase [15]. At the higher coverage of 0.50 ML, associated with the c(4x2)-CO phase, the two inequivalent hollow sites are occupied with equal probability [16]. Here we find, in

the presence of the coadsorbed hydrocarbon fragment, that both hollow sites are occupied, a result that may be taken to infer that the C_3H_3 blocks at least some of the preferred fcc hollows for CO adsorption. Comparisons of the quantitative structural parameter values obtained here with those of the earlier work on the pure CO adsorption phases (Table 1) also fail to show any really significant trends. As in the earlier studies, the precision on the C-O bondlength is too poor for variations in the individual values to be significant. The sensitivity of the C 1s PhD data to the C-O distance is poor, because this bondlength only influences these data through intramolecular multiple scattering, which is weak. Additional O 1s PhD structural analysis would substantially improve this precision, but in the present case the O 1s data proved unusable due to the strong overlap with the substrate emission. Most of the C-Pd bondlengths, $d_{C\text{-}1}$ also show variations that fall within the range defined by the (much higher) estimated precision. The only difference that is marginally significant (0.13±0.08 Å) is in the height of the C atom above the hcp hollow site (and the resulting bondlength). In this regard it is interesting that the interlayer spacings of the C atoms and the outermost Pd layer for the fcc site is also larger in the c(4x2) phase than in the lower coverage phase in which only the fcc hollow sites are occupied. Our results actually correspond more closely to the smaller interlayer spacings found in this lower-coverage pure CO phase, perhaps further suggesting that the co-occupation of the two hollows in our surfaces arises from fcc site blocking by the C_3H_3 species, rather than by CO. Indeed, in the pure c(4x2)-CO phase (coverage 0.50 ML) both the increased C-Pd bondlengths and the co-occupation of the two hollow sites may be attributable to CO-CO repulsive interactions that are not present in the case of the coadsorption phase studied here. In our coadsorption phase the CO coverage is certainly much lower. Our analysis of PhD and NEXAFS data from the intact furan adsorption phase shows the molecular plane to be essentially parallel to the surface [27], and in this case simple close-packing considerations using the atomic van der Waals radii [28] indicates that the maximum coverage is ~0.11 ML. The dissociation on heating actually leads to little change in the total C 1s photoemission intensity, so we may surmise that the coverage of both CO and C_3H_3 is ≤~0.1 ML.

Our results concerning the local adsorption site of the C_3H_3 species are less conclusive, in

that the PhD data alone fail to distinguish between two distinct models involving different local adsorption sites, although both preferred models are characterised by a molecular orientation near-parallel to the surface. We may therefore ask whether other considerations may provide a basis for establishing which of these two solutions is more likely to be correct. One possible basis for this is the local Pd-C nearest-neighbour bondlengths in the two structures. In model 5, the centre C atom occupies an off-atop site with a Pd-C bondlength of 2.12 Å, while the two outer C atoms are closer to hollow sites and have Pd-C bondlengths of 2.26 Å and 2.38 Å. In model 8 it is the outer two C atoms that are in off-atop sites, with Pd-C bondlengths of 2.11 Å, while the central C atom, closer to a hollow site, has a Pd-C nearest-neighbour bondlength of 2.31 Å. Comparison of the C_3H_3 species with the benzene molecule would lead us to expect that the outer C atoms have the capacity to form a stronger local C-Pd bond than the central C atom, which would seem to favour model 8; this model has significantly shorter C-Pd bonds at the outer C atoms. The actual chemisorption bondlengths may be compared with those formed by C_2H_2 [29] and C_6H_6 [30] coadsorbed with CO) on Pd(111), with values of 2.02 Å and 2.30 Å, respectively. These values actually fit rather well into this pattern. In the case of C_3H_3, we may anticipate that bonding of the outer C atoms to the surface could have a bond order of 1.5, if the C-C bonding retains the character of the C_6H_6 molecule, but could be lower if the intramolecular C-C bonding is strengthened. For adsorbed C_2H_2, on the other hand, the equivalent C-Pd bond order could be as large as 2, leading to a shorter chemisorption bondlength. These arguments, of course, neglect any possible formation of a local Pd-C_{centre} bond, perhaps inferred by the fact that this bondlength for model 8 is almost identical to that found for adsorbed benzene on Pd(111).

The possible bonding geometry of C_3H_3 has actually been considered previously in the STM study of the CO/C_3H_3 coadsorption phase on Pd(111), which included theoretical simulations of the STM images [10]. These calculations, however, did not include any structural optimisation, but assumed a geometry similar to that found in an organometallic carbonyl cluster compound in which a fully methylated C_3 species (i.e. $(CCH_3)_3$ rather than (CH_3)) is bonded to a triangular group of three Ru atoms [31]. The local geometry of the three C atoms of the C_3 species relative to the three Ru atoms in

this complex are shown in Fig. 8. Many aspects of this local geometry are similar to that found in the present study in model 8; in particular, the C_{outer}-Ru and C_{centre}-Ru bondlengths are 2.09 and 2.33 Å respectively, similar to the equivalent C-Pd bondlengths that we find of 2.11 and 2.31 Å, respectively. However, a rather significant difference is that in this cluster the C-C-C molecular plane is inclined to the Ru-Ru-Ru plane by 63°, very different from our value of 3°. In terms of the geometry, this difference can be attributed to the fact that the outer C atoms are actually quite close to bridging sites on the Ru_3 cluster, and thus significantly further from the atop geometry than we find in our structure determination on Pd(111). Of course, the bonding to three isolated Ru atoms is necessarily more local than the possible bonding to an extended surface plane of Pd atoms, so some difference is not particularly surprising.

In summary, we find that in the CO/C_3H_3 coadsorption phase on Pd(111), resulting from decomposition of adsorbed furan, the CO molecules occupy local sites and with local bondlengths essentially indistinguishable from those occupied at high coverage in the absence of the coadsorbed hydrocarbon fragment. By contrast, there is no prior information on the adsorption geometry of a C_3H_3 on any surface, and our PhD structure determination provides strong evidence for an adsorption geometry in which the molecular plane lies almost parallel to the metal surface. Formally, the PhD analysis fails to distinguish between two distinct local adsorption sites, but consideration of the resulting chemisorption bondlengths appears to favour a geometry in which the two outer C atoms bond in off-atop sites with the molecule as a whole centred close to three-fold coordinated hollow sites. A density-functional theory investigation of the adsorption energetics and geometry of this species may throw further light on the character of the associated chemisorption bonding.

Acknowledgements

The authors acknowledge the financial support of the Physical Sciences and Engineering Research Council (UK) and the award of beamtime at the BESSY II facility.

Table 1 Structural parameter values for the best-fit structure of CO on Pd(111) when coadsorbed with C_3H_3, compared with earlier results for pure CO adsorption phases on Pd(111). Interlayer spacings are denoted by *z*, interatomic bondlengths by *d*. Suffices define the atoms concerned, with the outermost and second substrate (Pd) atoms being labelled 1 and 2.

Parameter	CO + C_3H_3 coadsorption (this study)	c(4x2)-CO [16]	(√3x√3)R30º-CO [15]
$z_{C\text{-}1(fcc)}$ (Å)	1.25±0.05	1.31±0.06	1.27±0.05
$z_{C\text{-}O(fcc)}$ (Å)	1.23±0.15	1.14±0.12	1.25±0.13
$d_{C\text{-}1(fcc)}$ (Å)	2.02±0.03	2.06±0.04	2.03±0.04
$z_{C\text{-}1(hcp)}$ (Å)	1.24±0.05	1.37±0.06	-
$z_{C\text{-}O(hcp)}$ (Å)	1.31±0.16	1.14±0.14	-
$dz_{C\text{-}1(hcp)}$ (Å)	2.02±0.03	2.10±0.04	-
$z_{1\text{-}2}$ (Å)	2.20±0.10	-	-

Table 2 Summary of the results of the initial optimisation of the structural models for C_3H_3 on Pd(111) illustrated in Fig. 4

Model number	*R*-factor	$d_{C\text{-}C}$ (Å)	$\theta_{C\text{-}C\text{-}C}$ (º)
1	0.31	1.47	90.7
2	0.44	1.37	95.0
3	0.54	1.40	113.3
4	0.30	1.67	130.2
5	0.20	1.44	112.6
6	0.20	1.50	101.8
7	0.20	1.50	98.7
8	0.20	1.50	97.7

Table 3 Optimised structural parameter values for the two best-fit models for the local adsorption geometry of C_3H_3 on Pd(111) as determined by PhD. The labelling conventions are similar to those of Table 1, but with the added parameters, *xy*, defining the lateral offset of the relevant C atom from a site atop a surface Pd atom, $\theta_{C\text{-}C\text{-}C}$, denoting the intramolecular bond angle and, $\theta_{C2v\text{-}\perp}$, the tilt of the C_{2v} symmetry axis within the molecular plane relative to the surface normal.

Parameter	Model 5	Model 8
$z_{C(centre)\text{-}1}$ (Å)	2.09±0.04	2.03±0.11
$z_{C(outer)\text{-}1}$ (Å)	2.07, 1.93±0.05	2.07±0.04
$xy_{C(centre)}$ (Å)	0.38±0.10	1.10±0.11
$xy_{C(outer)}$ (Å)	1.17±0.06	0.40±0.07
$d_{C(centre)\text{-}1}$ (Å)	2.12±0.04	2.31±0.12
$d_{C(outer)\text{-}1}$ (Å)	2.38, 2.26±0.06	2.11±0.04
$d_{C\text{-}C}$ (Å)	1.45, 1.46±0.06	1.49±0.06
$\theta_{C\text{-}C\text{-}C}$ (°)	117±6	102±6
$\theta_{C2v\text{-}\perp}$ (°)	83±4	87±7

Figure Captions

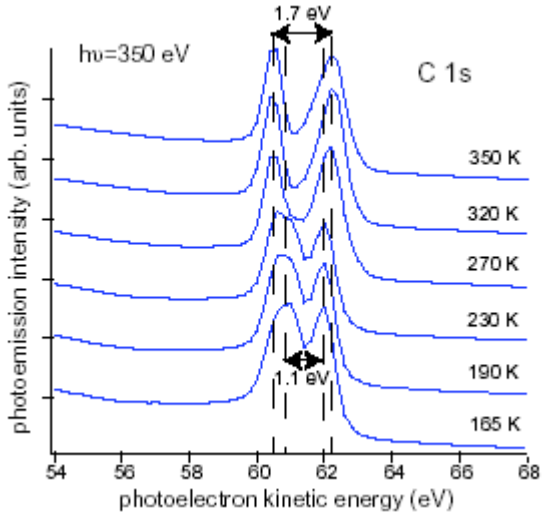

Fig. 1 C 1s spectra from Pd(111) after dosing with furan at low temperature and subsequently heating to various temperatures.

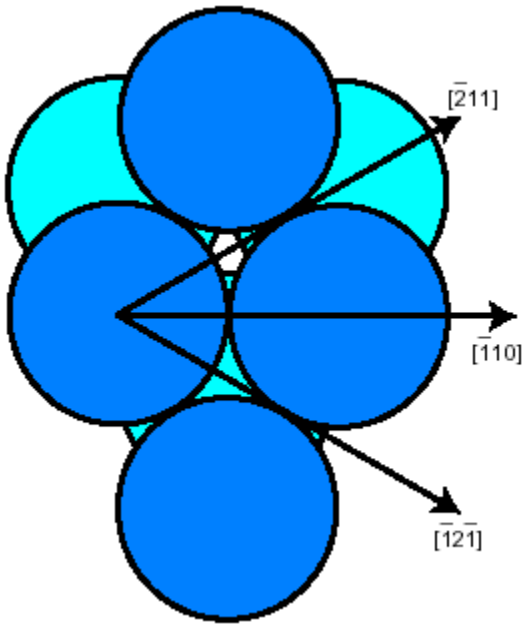

Fig. 2 Schematic plan view of the outermost two layers of a Pd(111) surface showing the definition of the high-symmetry azimuths used in the collection of the PhD data.

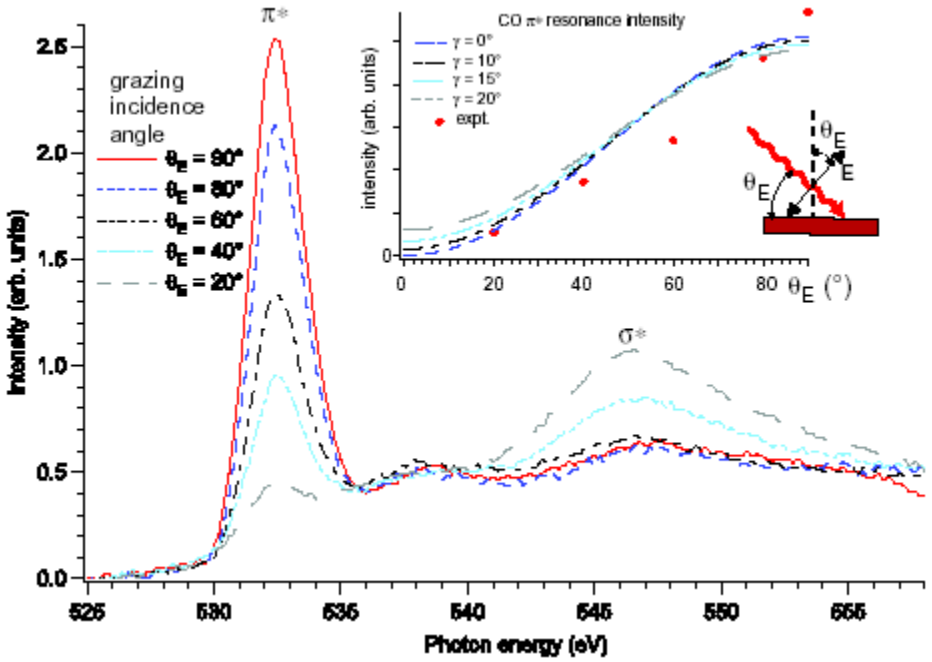

Fig. 3 O K-edge NEXAFS recorded from CO coadsorbed with C_3H_3 on Pd(111), at different grazing incidence angles, θ_E (as defined in the diagram). The inset shows the variation of the intensity of the π* resonance as a function of grazing incidence angle, compared with the theoretical models for several different orientations of the C-O axis relative to the surface normal.

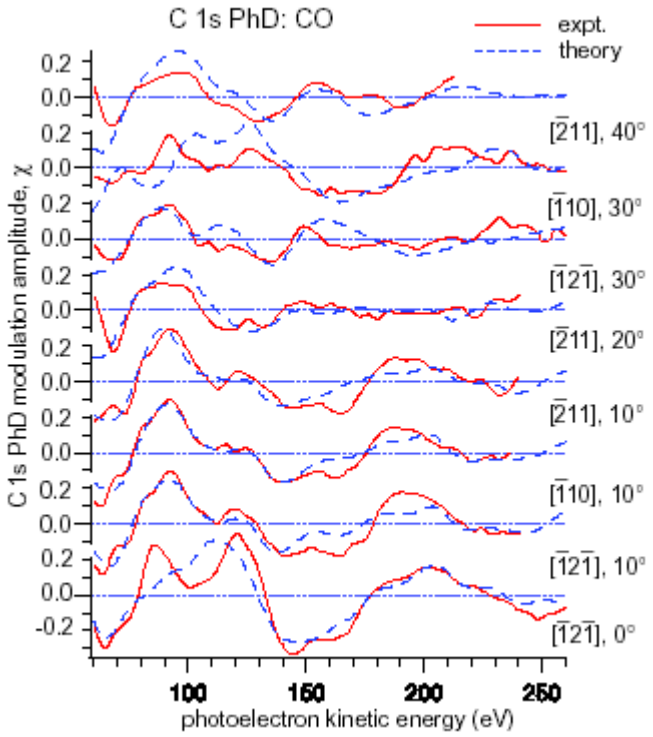

Fig. 4. Comparison of the experimental C 1s PhD modulation spectra obtained from the CO species, in the CO/C_3H_3 coadsorption phase on Pd(111), with the results of the multiple scattering simulations for the best-fit structural model involving equal occupation of fcc and hcp hollow sites.

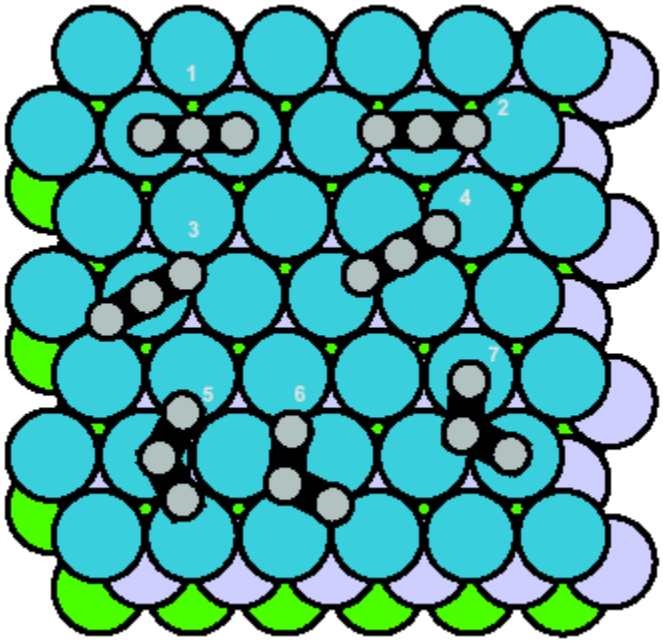

Fig. 5 Initial structural models tested for the location of the three C atoms in the C_3H_3 species on Pd(111), as described more fully in the text. Model 8, discussed in the text, corresponds to equal occupation of models 6 and 7 with identical structural parameters relative to the outermost Pd atom layer.

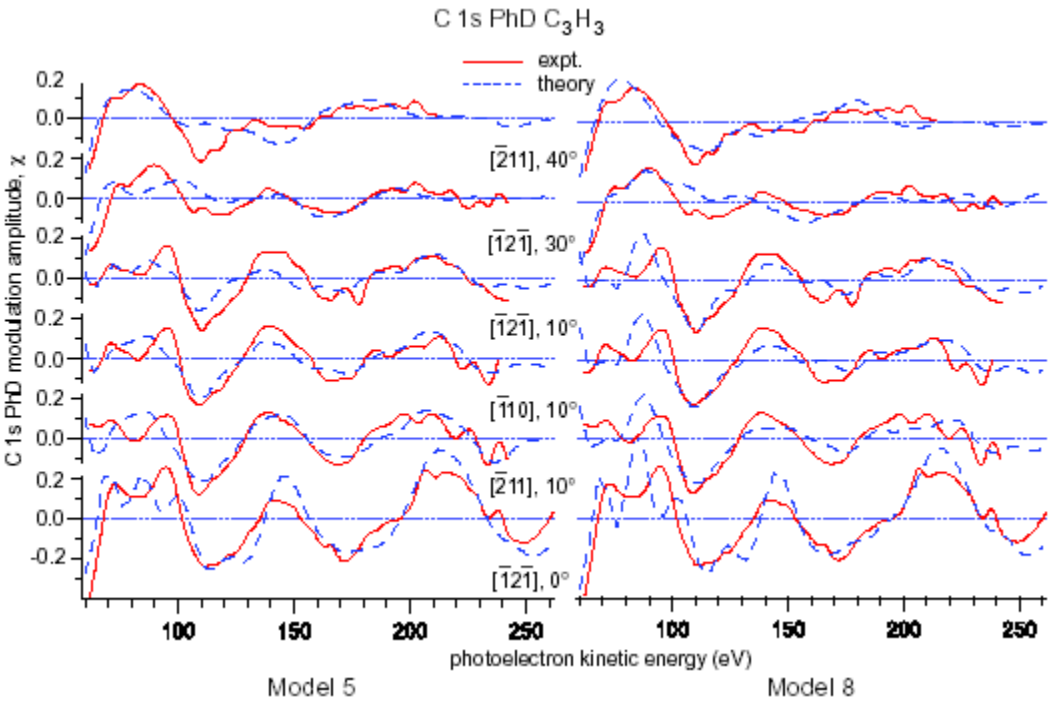

Fig. 6 Comparison of the experimental C 1s PhD modulation spectra obtained from the C_3H_3 species, in the CO/C_3H_3 coadsorption phase on Pd(111), with the results of the multiple scattering simulations for the two best-fit structural models.

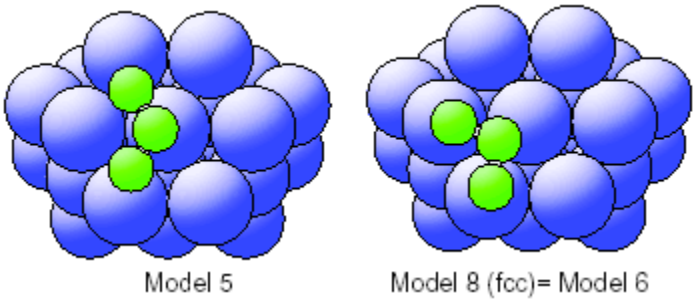

Fig. 7 Schematic diagrams of plan views of the two alternative structural models of the local geometry of C_3H_3 on Pd(111) as determined by the PhD investigation. The H atoms are omitted as the location of these weakly-scattering atoms cannot be determined experimentally. Note that model 8 actually assumes equal occupation of the two hollow sites (sites 6 and 7 of Fig. 5); here only that located near the fcc hollow (site 6) is shown.

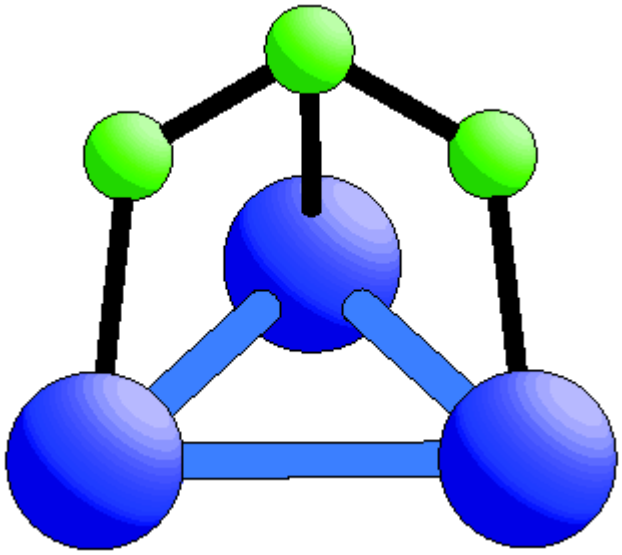

Fig. 8 Schematic diagram showing the local geometry of the three methylated C atoms of a $(CCH_3)_3$ species bonded to three Ru atoms in the organometallic complex $(\mu\text{-H})Ru_3(\mu_3\text{-}\eta^3\text{-CMeCMeCMe})(CO)_9$ [31].

References

1 D. P. Woodruff, *in Chemical Bonding at Surfaces and Interfaces* Eds. A. Nilsson, L. Pettersson, J. Nørskov, (Elsevier, Amsterdam, 2007) p1

2 U. Starke, A. Barbieri, N. Materer, M. A. Van Hove, G. A. Somorjai, Surf. Sci. 286 (1993) 1

3 A. Wander, M. A. Van Hove, G. A. Somorjai, Phys. Rev. Lett. 67 (1991) 626

4 E. Furimsky, Catal. Rev. Sci. Eng. 25 (1983) 421

5 R. M. Ormerod, C. J. Baddeley, C. Hardacre, R. M. Lambert, Surf. Sci. 360 (1996) 1

6 T. E. Caldwell, I. M. Abdelrehim, D. P. Land, J. Am. Chem. Soc. 118 (1996) 907

7 T. E. Caldwell, D. P. Land, J. Phys. Chem. B 103 (1999) 7869

8 D. N. Futaba, S. Chiang, J. Vac. Sci. Technol. A 15 (1997) 1295

9 A. Loui, S. Chiang, Appl. Surf. Sci. 237 (2004) 559

10 A. Loui, PhD. Thesis, University of California at Davis, 2005 (available as UMI Microform 3171896)

11 D. P. Woodruff, A. M. Bradshaw Rep. Prog. Phys. 57 (1994) 1029

12 D. P. Woodruff, Surf. Sci. Rep. 62 (2007) 1

13 K. J. S. Sawhney, F. Senf, M. Scheer, F. Schäfers, J. Bahrdt, A. Gaupp, W. Gudat, Nucl. Instrum. Methods A 390 (1997) 395

14 T. E. Caldwell, D. P. Land, Polyhedron 16 (1997) 3197

15 V. Fernandez, T. Gieβel, O. Schaff, K-M. Schindler, A. Theobald, C. J. Hirschmugl, S. Bao, A. M. Bradshaw, C. Baddeley, A. F. Lee, R. M. Lambert, D. P. Woodruff, V. Fritzsche, Z. phys. Chemie 198 (1997) 73

16 T. Gieβel, O. Schaff, C. J. Hirschmugl, V. Fernandez, K. -M. Schindler, A. Theobald, S. Bao, W. Berndt, A. M. Bradshaw, C. Baddeley, A. F. Lee, R. M. Lambert, D. P. Woodruff, Surf.Sci. 406 (1998) 90

17 J. Stöhr, R. Jaeger, Phys. Rev. B 26 (1982) 4111

18 J. Stöhr, *NEXAFS Spectroscopy*, Springer-Verlag, Berlin, 1977.

19 R.Davis, R.Toomes, D.P.Woodruff, O.Schaff, V.Fernandez, K.-M.Schindler, Ph.Hofmann, K.-U.Weiss, R.Dippel, V.Fritzsche and A.M.Bradshaw Surf.Sci. 393 (1997) 12

20 T.Gieβel, O.Schaff, C.J.Hirschmugl, V.Fernandez, K.-M.Schindler, A.Theobald, S.Bao, W.Berndt, A.M.Bradshaw, C.Baddeley, A.F.Lee, R.M.Lambert and D.P.Woodruff, Surf. Sci. 406 (1998) 90

21 V. Fritzsche, J.B. Pendry, Phys. Rev. B 48 (1993) 9054

22 V. Fritzsche, J. Phys.: Condens. Matter 2 (1990) 1413

23 V. Fritzsche, Surf. Sci. 265 (1992) 187

24 V. Fritzsche, Surf. Sci. 213 (1989) 648

25 J. B. Pendry, J. Phys.C: Solid State Phys. 13 (1980) 937

26 N. A. Booth, R. Davis, R. Toomes, D. P. Woodruff, C. Hirschmugl, K.-M. Schindler, O. Schaff, V. Fernandez, A. Theobald, Ph. Hofmann, R. Lindsay, T. Giessel, P. Baumgärtel, A. M. Bradshaw, Surf. Sci. 387 (1997) 152

27 M. J. Knight, F. Allegretti, E. A. Kröger, M. Polcik, C. L. A. Lamont, D. P. Woodruff, Surf. Sci. submitted for publication

28 J. L. Solomon, R. J. Madix, J. Stöhr, J. Chem. Phys. 94 (1991) 4012

29 C. J. Baddeley, A. F. Lee, R. M. Lambert, T. Gieβel, O. Schaff, V. Fernandez, K.-M. Schindler, A. Theobald, C. J. Hirschmugl, R. Lindsay, A. M. Bradshaw, D. P. Woodruff, Surf. Sci. 400 (1998) 166

30 A. Barbieri, M.A. Van Hove, G. A. Somorjai, Surf. Sci. 306 (1994) 261

31 M. R. Churchill, L. A. Buttrey, J. B. Keister, J. W. Ziller, T. S. Janik, W. S. Striejewske, Organometallics, 9 (1990) 766